Heliyon 10 (2024) e37121

Contents lists available at ScienceDirect

Heliyon

journal homepage: www.cell.com/heliyon

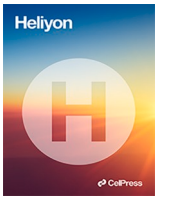

Research article

A 3D-Printed helmet for precise and repeatable neuromodulation targeting in awake non-human primates

Chengjie Tang [a], Wenlei Zhang [a], Xiaocheng Zhang [b], Jiahui Zhou [a], Zijing Wang [a], Xueze Zhang [d], Xiaotian Wu [a], Hang Su [a], Haifeng Jiang [a], Rongwei Zhai [b,**], Min Zhao [a,c,*]

[a] *Shanghai Mental Health Center, Shanghai Jiao Tong University School of Medicine, Shanghai, China*
[b] *Lingang Laboratory, Shanghai, China*
[c] *Shanghai Key Laboratory of Psychotic Disorders, Shanghai, China*
[d] *Academy for Engineering & Technology, Fudan University, China*

ARTICLE INFO

Keywords:
Non-invasive brain stimulation
Non-human primates
Transcranial magnetic stimulation
Target localization
Neuromodulation

ABSTRACT

The application of non-invasive brain stimulation (NIBS) in non-human primates (NHPs) is critical for advancing understanding of brain networks and developing treatments for neurological diseases. Improving the precision of targeting can significantly enhance the efficacy of these interventions. Here, we introduce a 3D-printed helmet designed to achieve repeatable and precise neuromodulation targeting in awake rhesus monkeys, eliminating the need of head fixation. Imaging studies confirmed that the helmet consistently targets the primary motor cortex (M1) with a margin of error less than 1 mm. Evaluations of stimulation efficacy revealed high resolution and stability. Additionally, physiological evaluations under propofol anesthesia showed that the helmet effectively facilitated the generation of recruitment curves for motor area, confirming successful neuromodulation. Collectively, our findings present a straightforward and effective method for achieving consistent and precise NIBS targeting in awake NHPs, potentially advancing both basic neuroscience research and the development of clinical neuromodulation therapies.

1. Introduction

Over the past three decades, non-invasive brain stimulation (NIBS) techniques have become indispensable tools for understanding cognitive brain networks and exploring therapies for neurological and mental diseases. Established techniques such as transcranial magnetic stimulation (TMS), transcranial electric stimulation (tES), and transcranial focused ultrasound stimulation (tFUS) have shown great potential in treating conditions such as stroke [1], Alzheimer's disease [2], depression [3], substance use disorder [4]. However, the effectiveness of these treatments varies. Further research into mechanisms and parameters of NIBS can help refine existing protocols to achieve better therapeutic outcomes. Precise and repeatable targeting of the treatment site is essential to better understand and optimize the stimulation effects. For example, the response rate of repetitive TMS (rTMS) in Major Depressive Disorder (MDD) patients increased with personalized targeting methods, highlighting the importance of precise targeting [5].

* Corresponding author. Shanghai Mental Health Center, Shanghai Jiao Tong University School of Medicine, Shanghai, China.
** Corresponding author.
E-mail addresses: zhairw@lglab.ac.cn (R. Zhai), drminzhao@smhc.org.cn (M. Zhao).

https://doi.org/10.1016/j.heliyon.2024.e37121
Received 2 July 2024; Received in revised form 15 August 2024; Accepted 28 August 2024
Available online 29 August 2024

Non-human primates (NHPs) are considered ideal models for studying NIBS [6], due to their high degree of anatomical and functional homology to human, the feasibility of combining electrophysiological recording, and their ability to perform more complex behaviors compared to rodents. Image-based neuro-navigating systems [7,8] are now widely used in NHPs to localize specific regions based on individual MRI images through a subject-image co-registration procedure using facial or cranial landmarks. However, this method has limitations. Neuro-navigation relies on head fixation, traditionally achieved by implanting a titanium headpost, an invasive procedure that may affect stimulation efficiency. Although minimal target error can be ensured in each session, it is challenging to confirm whether the same site is targeted across different sessions. Therefore, there is a need for better methods to achieve precise and stable positioning in NHPs without the requirement for headpost implantation.

Here, we introduce a 3D-printed customized helmet for NHPs, designed to be fixed with small fixtures implanted in the skull. This helmet system offers several advantages: 1) it ensures that the stimulator (TMS coil in this study) remains precisely at the same site and angle for each session without the need for a navigation system, 2) it significantly reduces costs due to the affordability of 3D printing, and 3) it minimizes trauma and allows for head movement in the animals by eliminating the need for headposts. This innovative approach has the potential to enhance the precision and repeatability of NIBS targeting in awake NHPs, paving the way for more effective research and therapeutic applications.

2. Materials and methods

2.1. Subjects

All experimental procedures were carried out in accordance with the guidelines and regulations of the Animal Care Committee of the Institute of Neuroscience and Centre for Excellence in Brain Science and Intelligence Technology, Chinese Academy of Sciences. Animal care protocols aligned with the US National Institutes of Health Guide for the Care and Use of Laboratory Animals. We utilized two adult male rhesus monkeys (M4 and M10) for the study. M4 (12 yrs) was weighed about 10 kg and M10 (10 yrs) 6 kg during the experiment. The monkeys were trained to sit in a primate chair (Suzhou Monkey Animal Experimental Equipment Technology Co, Jiangsu). They were provided with sufficient monkey chow in the morning and afternoon to maintain a healthy body weight. Fruit was given at noon unless otherwise noted, and water was continuously available throughout the day. The monkeys were individually housed in stainless steel cages with visual, auditory and olfactory contact with other monkeys. Toys were also provided in their cages, and videos were played once or twice a week in the animal housing rooms to provide additional environmental enrichment. The monkeys were maintained under a 12-h light–dark cycle (lights on from 07:00 a.m. to 19:00 p.m.).

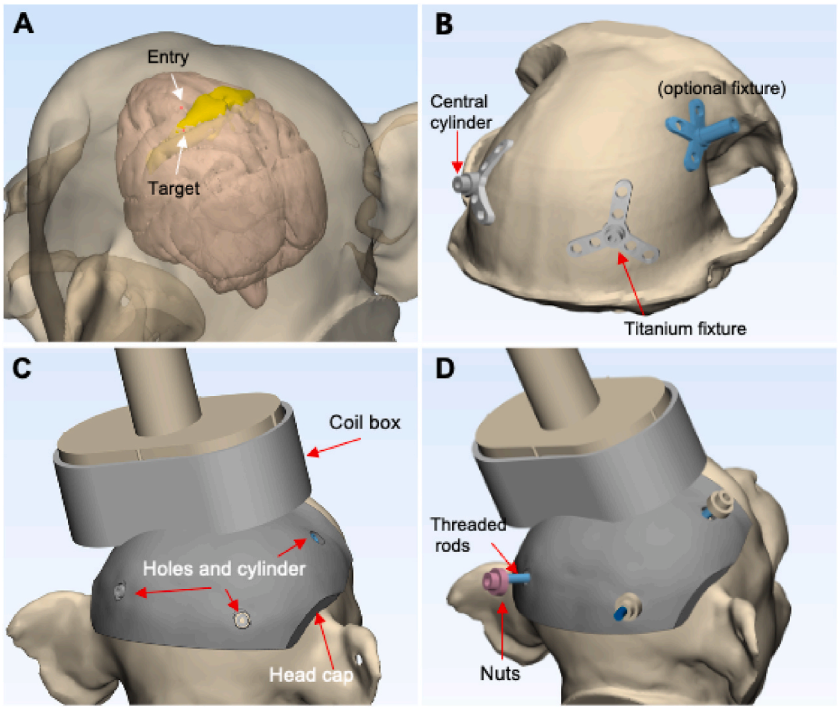

Fig. 1. The design of helmet. (A) The target in M1 area and its corresponding entry on the scalp. **(B)** Titanium fixtures fit onto the skull, featuring a central cylinder that contains internal threading. **(C)** A schematic diagram of a monkey wearing the helmet. The helmet is composed of coil box and head cap with holes for the cylinder of fixtures. The TMS coil is placed in the coil box. **(D)** Threaded rods are screwed in to the cylinder and nuts are screwed for fixation.

2.2. Helmet design

The helmet primarily consists of two components: a head cap that conforms to the scalp with perforations at corresponding positions to secure it to the fixtures on monkey's head, and a box for positioning the magnetic coil, ensuring that its center aligns with the target site. The fabrication process is as follows (Fig. 1): First, design titanium fixtures to be implanted in skull of the monkeys. These fixtures, resembling small-sized headposts, are intended to securely fix the helmet to the monkey's head. After surgical implantation, a postoperative computed tomography (CT) scan is obtained to confirm the position of the fixtures. The head cap is then customized to fit the monkeys' scalps, with corresponding holes drilled at the designated locations of the fixtures. Concurrently, the placement of the magnetic coil is designed based on magnetic resonance imaging (MRI) images to identify the target location. We provide detailed descriptions of each step in the following sections.

2.2.1. Modelling of fixtures

The fixtures are customized titanium intracranial implants for the monkeys (Fig. 1 B). To generate 3D models of the brain and skull, CT scans were acquired using a NeuroLogica scanner (NL3000, Ceretom). For anesthesia, atropine (0.05 mg/kg, i.m.) was administered first. Fifteen minutes later, Zoletil 50 (mixture of tiletamine and zolazepam, 4 mg/kg, i.m.) was then administered. The image data was imported into Mimics 20.0 (Materialise) and a model of the skull was generated through thresholding and segmentation, with the software's preset "bone" threshold option (threshold value range of 226–3071). We also performed smoothing and warping to reduce the triangular surfaces (below 5000) of the model, which helps prevent the design software from crashing due to overly complex models. The STereoLithography (STL) format of the skull model was exported and then imported in SolidWorks 2021. The fixture draft was designed in SolidWorks on a new plane above the estimated implant position on the skull. The fixture had three legs, each with one or two screw holes for screws, and a cylinder in the center with internal threading (thread size: M3). The length of the cylinder was determined by the thickness of the monkey's skin, ideally exposing the head by 2–3 mm. Then the bottom plane of the fixture was fitted to individual curvature of the monkey's skull with the command "extrude to body" [9]. The placement and number of the fixtures can be determined based on the size of the monkey's skull, the experiments planned for the future or other factors. Generally, to accommodate the TMS coil and allow for future electrode implantation without obstruction, the position of the fixtures should avoid the frontal-parietal region. Based on the structure of monkey's skull, for Monkey 4 with larger and more rounded skull, we customized three fixtures for it to enhance the stability of helmet fixation, with two placed at the rear and one secured at the right anterior side (Fig. 1B). For Monkey 10 with smaller and flatter skull, we designed two fixtures. After the modeling process, the titanium fixtures were fabricated using metal 3D printing technology.

2.2.2. Surgical procedure

Anesthesia was induced with intramuscularly administered atropine (0.05 mg/kg) and Zoletil 50 (mixture of tiletamine and zolazepam, 4 mg/kg, 15 min after atropine administration), and maintained with 1∼1.5 % isoflurane. The animal's head was secured in a stereotaxic frame. During the surgery, heart rate, external blood pressure, SpO2, CO2, temperature and respiration were continuously monitored. The titanium fixtures were autoclaved to ensure sterility. At the appropriate locations where the fixtures were to be placed, suitable-sized incisions were made in the skin. Tissues and muscles were separated, and the surface of the skull was cleaned using a bone curette and then rinsed with saline solution. It should be noted that the muscle was not removed; instead, it was carefully separated along its natural fibers at the necessary locations. The fixtures were placed on the skull and adjusted to fit perfectly against it. We used 2.7*4 mm Ti cortex screws to secure the fixtures to the bone. After that, the incision margins were sutured together, covering the legs of the fixture, leaving only the central cylinder exposed outside the skin. Ceftriaxone sodium was administered postoperatively to reduce the risk of infection. The monkeys were given one week to recover after surgery. After each day's experiment, povidone-iodine disinfection was performed around the fixtures.

2.2.3. Targeting and modelling of the helmet

To identify the target site, an MRI scan was conducted for clear visualization. T1-weighted image data were acquired on a 3-T whole-body scanner (Trio, Siemens Healthcare, Erlangen, Germany) with a custom-built 8-channel phased-array transceiver coil designed for animal imaging before the surgical operation. The standard atlas NMT 2.0 (https://prime-re.github.io) for rhesus monkeys was registered to individual's T1 image using ANTs (Advanced Normalization Tools) with the function "antsRegistrationSyN", and target site was located based on the standard atlas (Fig. 1 A). The entry site on the scalp was calculated using LOCALITE TMS Navigator. The post-operative CT image was registered to the T1 space as well.

To create the helmet, we first designed a fitted box for the TMS coil in SolidWorks (Fig. 1 C). Then it was imported into 3-matic (Materialise) in the format of STL. The 3D model of the post-operative head was also generated in 3-mtaic, and the target site and entry site were marked with points. Next, we created the head cap with a thickness of 4 mm, conforming to the curvature of the scalp using the operations "offset" and "Boolean". Screw holes at the positions of the fixture cylinder were drilled in the cap. The center point of the coil box was aligned with the entry point to ensure that the center of the coil corresponded directly to the target point to be stimulated with the align function in 3-matic. The coil box was positioned at an angle of about 45° to the midline [10]. To change the stimulation target, we simply adjust the position of the coil box. The bottom of the coil box and the relevant area of the head cap were removed to allow the coil to make direct contact with the scalp. The head cap and coil box were then merged into one helmet as a whole. The sharp edges were smoothed out. After modelling, the helmet was 3D-printed with ABS (Acrylonitrile-Butadiene-Styrene) -like resin.

2.3. Wearing the helmet

The monkeys sat in the primate chair. To safely and quickly fit the helmet on awake monkeys, we slightly restricted their movements. We made a thermoplastic mask with the method proposed by Drucker [11] but made some adjustments: we used a 3D-printed head as the model and created a relatively loose-fitting mask to accommodate all monkeys. After mildly restricting the movement of the monkey's head, we placed helmet on the head and aligned the two holes with the protruding fixture cylinders (Fig. 1 C). Threaded rods with an external M3 thread were screwed into the cylinder of the fixture. Next, nuts were threaded onto the threaded rod to secure the helmet in place (Fig. 1 D). The coil then can be placed into the coil box and secured with Velcro strips. The coil was simultaneously suspended using elastic cords to prevent any strain on the monkey's head. Once the helmet and coil were secured, the thermoplastic mask was removed, allowing the monkey to move their heads freely while wearing the helmet.

2.4. Target error validation

To verify the helmet's accuracy in precisely locating the target, we fabricated a validation helmet (Supplemental Fig. 1). Using the line connecting the entry and target points as the axis (Fig. 1 A), we generated an elongated cylinder on the head cap. The monkey wore the validation helmet for a CT scan, following the same anesthesia procedure as described above. 3D model was constructed and registered to the same space. The central axis of the helmet cylinder represents the actual stimulation location. The axis connecting the entry and target points represents the ideal trajectory. Measuring the intersection of these two axes on the scalp provides the target error. Error testing was performed three times on each monkey: before the start of the M1 stimulation experiment, mid-experiment, and post-experiment.

2.5. M1 stimulation with TMS

We used MagPro X100 magnetic stimulator (MagVenture, DK) and a butterfly-shaped coil Cool-B35 HO for animals for single pulse TMS stimulation. We stimulated the M1 area of the monkeys in both awake and anesthetized states. To assess the accuracy and spatial resolution of the helmet, we selected different targets. Previous study has demonstrated that the cortico-motoneuron cells responsible for movements below the forearm are located between the spur of the arcuate sulcus and the superior precentral sulcus, spanning approximately 6–7 mm [12,13] and motor evoked potential (MEP) amplitudes generated by stimuli within 0.5 cm radius of a specific hand muscle hotspot exhibit notable similarity, indicating that increments larger than 0.5 cm may be requisite to discern alterations [14,15]. Based on these studies, we selected four targets along this axis, each approximately 5 mm apart. Coordinates and illustrations are shown in Fig. 2 and Supplemental Table 1. Each monkey was stimulated at four targets in the two states.

In the awake state, we observed hand muscle twitches following single-pulse stimulation of the M1 area, characterized by the number of visible muscle twitches out of 10 stimulations [16,17]. The monkeys sat in the primate chair and wore the helmet as described above. Before formal testing, the monkeys were allowed to be accustomed to the helmet and coil in the experimental room for one week. Each day, two target points were tested and each target was tested for 6 days. TMS intensity was documented as percent machine output (% MO) with 100 % corresponding to maximal electrical current conducted through the magnetic coil. The intensity was increased gradually by 1 % from low to high until muscle twitches were observed in all 10 stimulations. The intensity used in Monkey 4 was about 35%–50 %, and in Monkey 10 was about 20%–32 %. Two experimenters observed and recorded the results together to minimize subjective bias.

In the anesthetized state, we recorded the MEPs elicited from the flexor pollicis muscles. MEPs were monitored using the built-in MEP mode of MagPro X100. The monkey was sedated with ketamine (10 mg/kg, i.m.) and moved to the operation room. Anesthesia was maintained with propofol i.v. (10.5 mg/kg/h for Monkey 4 and 9 mg/kg/h for Monkey 10). During the experiment, heart rate, SpO2 and temperature were monitored continuously. The monkey was positioned laterally, and the hair on the contralateral forearm and wrist area to the stimulated brain region was shaved and depilated with depilatory cream. The skin and the palm were gently

Fig. 2. TMS stimulation at the M1 area. (A) The stimulation sites in the M1 region for Monkey 4. **(B–C)** Changes in finger twitching times when stimulating the M1 region at different sites using varying intensities. The dots represent the mean number of twitches across six sessions, and the color bands indicate the standard error. *p < 0.05, **p < 0.01, ***p < 0.001.

cleaned with alcohol. We inserted an acupuncture needle (0.35 mm) into the abductor pollicis brevis muscle (APB) as a recording electrode, and placed electrode patches on the back of the hand as reference electrode, wrist as ground electrode. Using acupuncture needles as recording electrodes can significantly reduce EMG signal noise. We controlled the background noise to below 20 μV. We started the experiment when the monkey lost the eyelid reflex and maintained a stable heart rate. Then we placed the helmet on the monkey and positioned the coil to prepare for testing. Single pulses were delivered at varying intensities in a randomized order, including 75 %, 80 %, 90 %, 95 %, 100 %, 105 %, 110 %, 120 %, 130 %, 140 % and 150 % of the baseline intensity, with a minimum 5 s inter-pulse interval [18,19]. The baseline intensity was defined as the strength required to elicit a about 100 μV MEP. The baseline was 55 % for Monkey 4 and 25 % for Monkey 10. At least 5 valid MEPs were collected at each intensity for averaging. If there was no response after 20 stimuli, the intensity was considered unable to evoke MEPs. The effect of posterior-anterior (PA) induced currents and anterior-posterior (AP) induced currents were both tested.

2.6. Statistical analysis

Statistical analyses were performed using R 4.3.2. We fitted a generalized linear mixed-effects model (GLMM) with a binomial distribution to assess whether the number of finger twitches was associated with the stimulation target and intensity. Sessions tested on different days were set as random effect. The formula is: twitching times/total times $\sim$ target + output% + 1 | session), followed by Turkey HSD test. To estimate the motor threshold (stimulation intensity for 5 finger twitches), we fitted a linear regression model with the formula: output $\sim$ twitching times + target. The stability of responses across different sessions was assessed using the coefficient of variation (CV) and the smallest real difference (SRD). $SRD_{95\ \%}$ ($1.96 \times SEM \times \sqrt{2}$) was used to determine whether the change score of an individual patient was real at the 95 % confidence level. SRD was then divided by the mean of all the measurements from both sessions and multiplied by 100 % to give a percentage value, the SRD percentage. SRD% <30 % of the mean score was used to determine whether the SRD is acceptable [20–23]. To analyze the effect of current direction on MEP peak amplitude, linear regression was performed: peak $\sim$ output% + direction. An independent two-sample *t*-test was used to analyze the difference in latency of MEP induced by different current directions.

3. Results

3.1. Targeting accuracy of the helmet

To evaluate the targeting accuracy of the 3D-printed helmet, the monkeys wore the validation helmet and underwent a CT scan. We measured the distance between the actual target and the planned target on the 3D images to determine the target error (see Methods). The results are summarized in Table 1. Each monkey underwent the validation procedure at three time points: before the start of TMS stimulation, during the experiment, and after the experiment. For Monkey 4, there was an 11-month gap between the first and third tests, while for Monkey 10, there was a 4-month gap. The average error across six tests conducted on two monkeys was 0.95 ± 0.20 mm (mean ± SD). This consistent targeting accuracy, with an error margin of less than 1 mm, demonstrates the reliability of the helmet in maintaining precise and repeatable neuromodulation targeting over extended periods and multiple sessions.

3.2. Resolution and stability of target localization with helmets

The response to stimulation of the primary motor cortex (M1) is typically used to determine thresholds and assess the stimulation efficacy. We created four helmets for four targets in the M1 area (see Methods), spaced approximately 5 mm apart along the longitudinal axis of M1 (Fig. 2A). These targets were located in left hemisphere of Monkey 4 and the right hemisphere of Monkey 10, with coordinates listed in Supplemental Table 1. Each target point was stimulated ten times, and the number of muscle twitches in the contralateral hand was observed, a method typically used to determine the resting motor threshold (rMT) [24].

The video (Supplemental Video) shows the monkey wearing the helmet. In both monkeys, stimulating targets 1, 2, and 3 elicited finger twitches at relatively low intensities (36 % in Monkey 4 and 21 % in Monkey 10; Fig. 2B and C), suggesting that these points, particularly target 1 and 2, were in close proximity to the hand hotspot. In contrast, stimulating target 4 required significantly higher intensities (GLMM model, $p < 2e\text{-}16$, details in Supplemental Tables 2 and 3), indicating that target 4 was further from the hotspot. These findings underscored the helmet's capability to deliver high-resolution performance.

Table 2 displays the predicted stimulation intensities required to induce five finger twitches (Linear regression, $R^2 = 0.8433$, $p < 2.2e\text{-}16$ for Monkey 4 and $R^2 = 0.8905$, $p < 2.2e\text{-}16$ for Monkey 10, details in Supplemental Table 4), providing an estimated motor threshold (eMT) for our monkeys (about 37 % in Monkey 4 and 23 % in Monkey 10). The stability of responses on different

Table 1
Target error in two monkeys.

Trials/Monkeys	Days post-operative for M4	Monkey 4	Days post-operative for M10	Monkey 10
1	14 days	0.83 mm	45 days	0.76 mm
2	238 days	0.94 mm	93 days	0.78 mm
3	371 days	1.15 mm	114 days	1.22 mm
Mean ± SD		0.97 ± 0.16 mm		0.92 ± 0.26 mm

experimental days (six sessions) was assessed at 95%–110 % eMT, as shown in Table 3. The CV values were all below 25 %, and the SRD% all below 30 % at the 110 % eMT, indicating relatively low variability.

Additionally, as the stimulation target approached the midline, muscle contractions were observed not only in the fingers but also in the wrist and forearm. These results indicated that, targeting M1 with the helmets could induce movements with a certain degree of stability and differentiate effects between different sites.

3.3. Application of helmets in investigating recruitment curves under propofol anesthesia

Motor evoked potentials (MEPs) provide a temporally precise and muscle-specific readout of the motor system, exhibiting different changes under pathological conditions [25]. Investigating the entire recruitment curve of MEPs at various stimulus intensities (input–output curves) offers a more comprehensive characterization of cortical excitability [20]. Halton established an NHP model for TMS studies of cortical excitability using isoflurane anesthesia [19]. In this study, we measured MEPs of abductor pollicis brevis (APB) in monkeys wearing helmets under propofol anesthesia, which is also commonly used in clinical settings for maintaining anesthesia. Helmets for target 1 were used for both monkeys. The average MEPs under propofol anesthesia are shown in Fig. 3A and B. We observed a lower probability of evoking MEPs at lower intensities (Fig. 3C and D). As the stimulation intensity increased, both the peak amplitude and the probability of evoking MEPs increased in both monkeys (Fig. 3A–D). The maximum peak value was approximately 400 μV in Monkey 4 and 300 μV in Monkey 10, likely influenced by the level of anesthesia.

We further investigated the differences in MEPs evoked between posterior-anterior (PA) and anterior-posterior (AP) currents. The threshold for neuron stimulation strongly depends on the current direction: axons are best stimulated by currents flowing nearly parallel to their main orientation [26]. When the coil is oriented to produce a PA current flow on motor cortex, the threshold is lowest. As expected, PA current induced MEPs with significantly greater amplitude and higher probability compared to AP current (Linear regression, $p = 0.002$ in Monkey 4, $p = 6.49e\text{-}11$ in Monkey 10), as shown in Fig. 3A–D. In Monkey 10, PA current also induced MEPs with a shorter latency (Fig. 3E, *t*-test, $p = 3.409e\text{-}13$).

4. Discussion

In this study, we developed a specialized helmet for use on awake non-human primates, enabling precise and stable targeting of neurostimulation sites. The average target error is within 1 mm, comparable to the error with neuro-navigation systems [27]. Applying the targeted M1 helmet, we successfully observed finger twitches and MEP peaks, confirming a functional resolution of approximately 5 mm and demonstrating good stability across sessions.

Our helmet system addresses several issues associated with traditional methods while ensuring accuracy. Regarding stimulation efficiency, the implantation of a headpost in the traditional method may affect the outcome in multiple ways: 1) Headposts are generally implanted in the frontal-parietal region. The placement angle of the coil is constrained by the need to coordinate with the headpost position. 2) Non-titanium cranial screws can interfere with the magnetic field induced by TMS. 3) If dental acrylic is used to reinforce the headpost, it will increase the trauma area around the post. This may occupy the scalp area corresponding to the target, requiring the coil to be placed on the dental cement and increasing the distance from the stimulation site to the target. In our design, since the fixtures are usually implanted away from the stimulation site, they do not obstruct the placement of the coil. Thus, the direction and angle of the coil can be freely adjusted. and the center of the coil is closely aligned with the animal's scalp without potential obstructions. As for animal welfare, headpost implantation surgery is traumatic, and the struggle of monkeys against head fixation brings secondary trauma. If dental acrylic is used, there is a risk of subsequent infection, which may require frequent debridement [28]. According to European Union 2013 regulation on non-human primate research and its firm Reduction and Refinement requests, we proposed this helmet system without headpost implantation. The small implanted fixtures maintained their integrity for at least for one year, with no occurrences of infection in our monkeys. Their heads could move freely during stimulation process.

Our method also reduces uncontrollable sources of error. Target error in the neuro-navigation system mainly comes from 1) movement of the reference marker during examinations, 2) subject-to-image registration error, and 3) coil localization [8]. In our helmet system, registration is not required, and the placement and angle of the coil are already integrated with the helmet. Therefore,

Table 2
Estimated motor threshold at different targets.

Animal	Target	eMT (%) (induce 5 finger twitches)	95 % CI
M4	1	37.65	37.16, 38.14
	2	37.94	37.44, 38.45
	3	39.42	38.97, 39.87
	4	46.03	45.59, 46.47
M10	1	23.95	23.66, 24.24
	2	23.63	23.34, 23.92
	3	24.91	24.64, 25.19
	4	28.70	28.38, 29.03

Table 3
Stability of responses across sessions in four targets of two monkeys.

Animal	Target	Output (%MO)	Mean	SEM	CV (%)	$SRD_{95\ \%}$	$SRD_{95\ \%}$ (%)
M4	1	95 % eMT	4.17	1.49	87.74	0.46	277.19
		100 % eMT	6.67	0.33	12.25	0.92	13.86
		105 % eMT	8.50	0.81	23.23	2.23	26.29
		110 % eMT	10.00	0.00	**0.00**	0.00	**0.00**
	2	95 % eMT	1.17	0.67	97.98	1.85	110.87
		100 % eMT	6.83	1.54	55.08	4.26	62.33
		105 % eMT	8.67	0.80	22.69	2.22	25.67
		110 % eMT	10.00	0.00	**0.00**	0.00	**0.00**
	3	95 % eMT	1.33	0.99	181.66	2.74	205.57
		100 % eMT	3.67	1.33	89.07	3.70	100.79
		105 % eMT	8.67	0.21	5.96	0.58	6.4
		110 % eMT	0.83	0.17	**4.15**	0.46	**4.70**
	4	95 % eMT	1.67	0.99	145.32	2.74	164.45
		100 % eMT	5.17	0.74	35.51	2.08	40.19
		105 % eMT	8.00	1.63	50.00	4.53	56.58
		110 % eMT	9.67	0.33	**8.45**	0.92	**9.56**
M10	1	95 % eMT	3.17	1.05	80.92	2.90	91.57
		100 % eMT	4.67	1.05	55.33	2.92	62.61
		105 % eMT	8.17	0.75	22.47	2.07	25.42
		110 % eMT	9.17	0.65	**17.48**	1.81	**19.78**
	2	95 % eMT	1.00	0.37	89.44	1.02	101.21
		100 % eMT	7.00	1.05	40.41	3.20	45.74
		105 % eMT	9.00	0.63	17.21	1.75	19.48
		110 % eMT	9.67	0.33	**8.45**	0.92	**9.56**
	3	95 % eMT	1.00	0.37	89.44	1.01	101.21
		100 % eMT	5.17	1.28	60.49	3.54	68.45
		105 % eMT	7.17	1.01	34.65	2.81	39.21
		110 % eMT	9.00	0.82	**22.22**	2.26	**25.15**
	4	95 % eMT	0.83	0.48	140.29	1.32	158.75
		100 % eMT	5.67	0.99	42.74	2.74	48.37
		105 % eMT	8.83	0.60	16.66	1.67	18.86
		110 % eMT	10.00	0.00	**0.00**	0.00	**0.00**

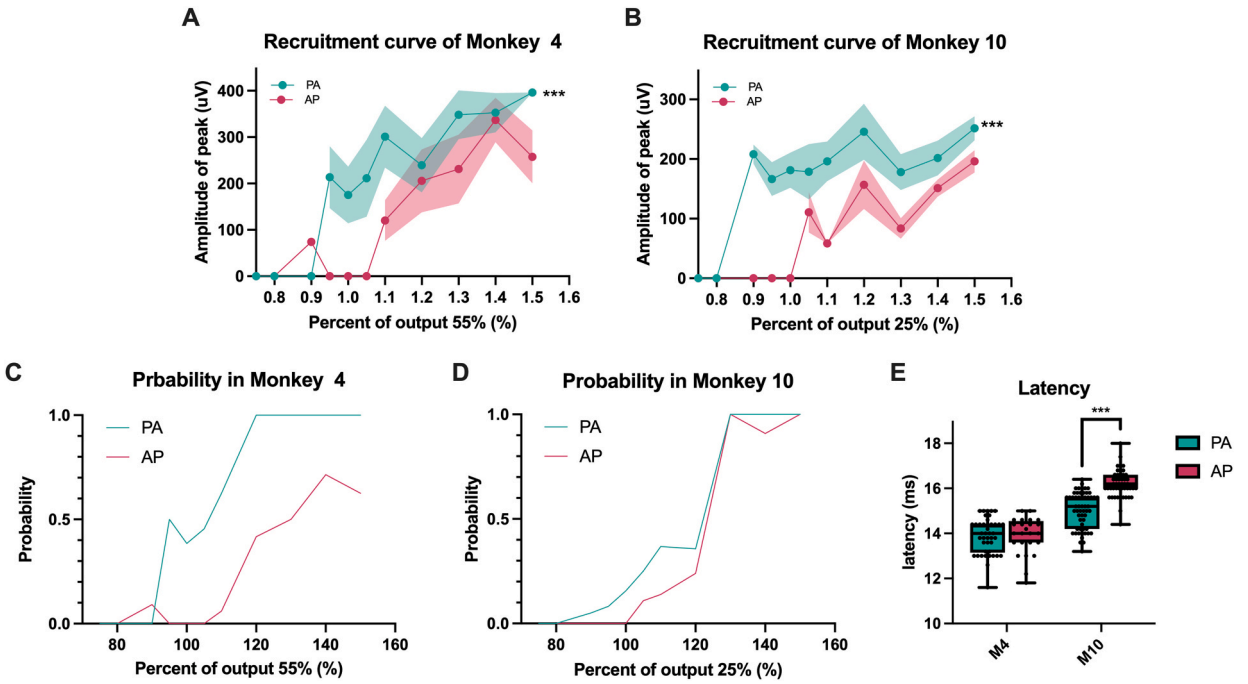

Fig. 3. Recruitment curves under propofol anesthesia. (A–B) Average MEPs recorded under propofol anesthesia in Monkey 4 and Monkey 10. **(C–D)** Probability of evoking MEPs at different stimulation intensities in both monkeys. **(E)** Comparison of MEP latency induced by PA and AP currents in the monkeys. Posterior to anterior current, PA; anterior to posterior current, AP. *p < 0.05, **p < 0.01, ***p < 0.001.

errors from the above steps are eliminated. Instead, the main sources of error are 1) 3D modeling of CT images, and 2) helmet placement. Our experimental results showed that the error increased after several months due to slight changes in the animal's head shape over (e.g., hair growth, fat changes), causing the helmet to no longer fit well. We recommended remanufacturing the helmet based on the latest imaging after a certain period.

Additionally, the helmet enables precise positioning without a neuro-navigation system, greatly saving the positioning time. The helmets are 3D printed using resin, resulting in low costs, approximately 40 CNY per helmet. When we need to change the target, we simply adjust the position of the coil box and reprint, offering relative flexibility. Although we made the helmets for TMS, a helmet for transcranial ultrasound can also be made based on the same principle. We believe that this helmet system, while ensuring precision, represents a better choice for neuromodulation localization in non-human primates.

We selected four sites along the long axis of the M1 region as TMS stimulation targets. Our results indicated that lower intensity stimulation of the more lateral targets (target 1 and target 2) could evoke greater finger twitches. We provided the coordinates of these two points on the standard atlas, suggesting that the area between them represents the hand hotspot region in rhesus monkeys. Our study also confirmed that the helmet has a functional resolution of at least 5 mm, which is rarely verified in other studies.

The stability of effects is crucial for neuromodulation. Several studies have measured the stability of MEPs over time, using SRD and intraclass correlation coefficient (ICC) as indicators of test-retest reliability [20–23]. Typically, an intensity of 110 % rMT is used, as it can evoke MEPs at 95 % probability and minimizes excessive current spread [29]. Our results also support that 110 % eMT could evoke stable responses in rhesus monkeys, while responses reach saturation (with a probability of 100 %) at 120 % eMT.

In our experiment, we did not directly compare our helmet system with commonly used neuro-navigation techniques because none of our monkeys were implanted with headposts. While determining the motor threshold, we did not measure MEPs in awake monkeys but rather observed the number of finer twitches, which only allowed us to estimate the motor threshold through modeling.

5. Conclusion

We have designed a 3D-printed helmet capable of precise and stable neural modulation targeting in awake non-human primates. It is cost-effective and causes less harm to the monkeys compared to headpost implants, which is favorable to animal welfare. Additionally, it can be adjusted to support various neural modulation devices. This approach facilitates more convenient and stable neural modulation research in non-human primates.

Ethics statement

The use and care of rhesus monkeys (*Macaca mulatta*) complied with the guidelines of the Animal Advisory Committee at the Center for Excellence in Brain Science and Intelligence Technology, Chinese Academy of Sciences. The ethics application entitled "Cognitive-behavioral and neural circuitry of non-human primate models of schizophrenia, novel gene editing techniques and animal models of brain disorders in non-human primates, cortical developmental mechanisms and non-human primate models of related diseases" (#ION-2017006) was approved by the Center for Excellence in Brain Science and Intelligence Technology (CEBSIT), Chinese Academy of Sciences.

Data availability statement

All experimental data included in this study can be obtained by contacting the authors if needed.

CRediT authorship contribution statement

Chengjie Tang: Writing – review & editing, Writing – original draft, Methodology, Investigation, Formal analysis, Conceptualization. **Wenlei Zhang:** Writing – review & editing, Investigation, Conceptualization. **Xiaocheng Zhang:** Investigation. **Jiahui Zhou:** Investigation. **Zijing Wang:** Investigation. **Xueze Zhang:** Methodology. **Xiaotian Wu:** Investigation. **Hang Su:** Writing – review & editing. **Haifeng Jiang:** Writing – review & editing. **Rongwei Zhai:** Writing – review & editing, Supervision, Resources, Methodology, Conceptualization. **Min Zhao:** Supervision, Resources, Funding acquisition.

Declaration of competing interest

The authors declare that they have no known competing financial interests or personal relationships that could have appeared to influence the work reported in this paper.

Acknowledgements

This work was supported by STI2030-Major Projects (2021ZD0202105 to H.F.J), Innovation of Science and Technology 2030-Major Project "platform of nonhuman primate models" (Grant No. 2021ZD0200900 to R.W.Z.), grants from Lingang Lab (LG202106-03 to M.Z. and R.W.Z.), National Nature Science Foundation (82130041 to M.Z.), and Shanghai Key Laboratory of Psychotic Disorders (13DZ2260500 to M.Z.)

Appendix A. Supplementary data

Supplementary data to this article can be found online at https://doi.org/10.1016/j.heliyon.2024.e37121.

References

[1] G. Di Pino, G. Pellegrino, G. Assenza, F. Capone, F. Ferreri, D. Formica, F. Ranieri, M. Tombini, U. Ziemann, J.C. Rothwell, V. Di Lazzaro, Modulation of brain plasticity in stroke: a novel model for neurorehabilitation, Nat. Rev. Neurol. 10 (2014) 597–608, https://doi.org/10.1038/nrneurol.2014.162.

[2] J. Teselink, K.K. Bawa, G.K. Koo, K. Sankhe, C.S. Liu, M. Rapoport, P. Oh, S. Marzolini, D. Gallagher, W. Swardfager, N. Herrmann, K.L. Lanctôt, Efficacy of non-invasive brain stimulation on global cognition and neuropsychiatric symptoms in Alzheimer's disease and mild cognitive impairment: a meta-analysis and systematic review, Ageing Res. Rev. 72 (2021) 101499, https://doi.org/10.1016/j.arr.2021.101499.

[3] E.J. Cole, A.L. Phillips, B.S. Bentzley, K.H. Stimpson, R. Nejad, F. Barmak, C. Veerapal, N. Khan, K. Cherian, E. Felber, R. Brown, E. Choi, S. King, H. Pankow, J. H. Bishop, A. Azeez, J. Coetzee, R. Rapier, N. Odenwald, D. Carreon, J. Hawkins, M. Chang, J. Keller, K. Raj, C. DeBattista, B. Jo, F.M. Espil, A.F. Schatzberg, K. D. Sudheimer, N.R. Williams, Stanford neuromodulation therapy (SNT): a double-blind randomized controlled trial, Aust. J. Pharm. 179 (2022) 132–141, https://doi.org/10.1176/appi.ajp.2021.20101429.

[4] M.C. Salling, D. Martinez, Brain stimulation in addiction, Neuropsychopharmacology 41 (2016) 2798–2809, https://doi.org/10.1038/npp.2016.80.

[5] P.B. Fitzgerald, Targeting repetitive transcranial magnetic stimulation in depression: do we really know what we are stimulating and how best to do it? Brain Stimul. 14 (2021) 730–736, https://doi.org/10.1016/j.brs.2021.04.018.

[6] S.J. Lehmann, B.D. Corneil, Completing the puzzle: why studies in non-human primates are needed to better understand the effects of non-invasive brain stimulation, Neurosci. Biobehav. Rev. 132 (2022) 1074–1085, https://doi.org/10.1016/j.neubiorev.2021.10.040.

[7] P. Pouget, S. Frey, H. Ahnine, D. Attali, J. Claron, C. Constans, J.-F. Aubry, F. Arcizet, Neuronavigated repetitive transcranial ultrasound stimulation induces long-lasting and reversible effects on oculomotor performance in non-human primates, Front. Physiol. 11 (2020) 1042, https://doi.org/10.3389/fphys.2020.01042.

[8] J. Ruohonen, J. Karhu, Navigated transcranial magnetic stimulation, Neurophysiologie Clinique/Clinical Neurophysiology 40 (2010) 7–17, https://doi.org/10.1016/j.neucli.2010.01.006.

[9] X. Chen, J.K. Possel, C. Wacongne, A.F. van Ham, P.C. Klink, P.R. Roelfsema, 3D printing and modelling of customized implants and surgical guides for non-human primates, J. Neurosci. Methods 286 (2017) 38–55, https://doi.org/10.1016/j.jneumeth.2017.05.013.

[10] S. Rossi, A. Antal, S. Bestmann, M. Bikson, C. Brewer, J. Brockmöller, L.L. Carpenter, M. Cincotta, R. Chen, J.D. Daskalakis, V. Di Lazzaro, M.D. Fox, M. S. George, D. Gilbert, V.K. Kimiskidis, G. Koch, R.J. Ilmoniemi, J.P. Lefaucheur, L. Leocani, S.H. Lisanby, C. Miniussi, F. Padberg, A. Pascual-Leone, W. Paulus, A. V. Peterchev, A. Quartarone, A. Rotenberg, J. Rothwell, P.M. Rossini, E. Santarnecchi, M.M. Shafi, H.R. Siebner, Y. Ugawa, E.M. Wassermann, A. Zangen, U. Ziemann, M. Hallett, Safety and recommendations for TMS use in healthy subjects and patient populations, with updates on training, ethical and regulatory issues: expert Guidelines, Clin. Neurophysiol. 132 (2021) 269–306, https://doi.org/10.1016/j.clinph.2020.10.003.

[11] C.B. Drucker, M.L. Carlson, K. Toda, N.K. DeWind, M.L. Platt, Non-invasive primate head restraint using thermoplastic masks, J. Neurosci. Methods 253 (2015) 90–100, https://doi.org/10.1016/j.jneumeth.2015.06.013.

[12] H.C. Kwan, W.A. MacKay, J.T. Murphy, Y.C. Wong, Spatial organization of precentral cortex in awake primates. II. Motor outputs, J. Neurophysiol. 41 (1978) 1120–1131, https://doi.org/10.1152/jn.1978.41.5.1120.

[13] J.-A. Rathelot, P.L. Strick, Muscle representation in the macaque motor cortex: an anatomical perspective, Proc. Natl. Acad. Sci. U.S.A. 103 (2006) 8257–8262, https://doi.org/10.1073/pnas.0602933103.

[14] R.E. Sondergaard, D. Martino, Z.H.T. Kiss, E.G. Condliffe, TMS motor mapping methodology and reliability: a structured review, Front. Neurosci. 15 (2021) 709368, https://doi.org/10.3389/fnins.2021.709368.

[15] A.A. de Goede, E.M. ter Braack, M.J.A.M. van Putten, Accurate coil positioning is important for single and paired pulse TMS on the subject level, Brain Topogr. 31 (2018) 917–930, https://doi.org/10.1007/s10548-018-0655-6.

[16] M.C. Romero, L. Merken, P. Janssen, M. Davare, Neural effects of continuous theta-burst stimulation in macaque parietal neurons, Elife 11 (2022) e65536, https://doi.org/10.7554/eLife.65536.

[17] A. Gerits, C.C. Ruff, O. Guipponi, N. Wenderoth, J. Driver, W. Vanduffel, Transcranial magnetic stimulation of macaque frontal eye fields decreases saccadic reaction time, Exp. Brain Res. 212 (2011) 143–152, https://doi.org/10.1007/s00221-011-2710-3.

[18] M. Hassanzahraee, M. Zoghi, S. Jaberzadeh, Longer transcranial magnetic stimulation intertrial interval increases size, reduces variability, and improves the reliability of motor evoked potentials, Brain Connect. 9 (2019) 770–776, https://doi.org/10.1089/brain.2019.0714.

[19] C.A. Hanlon, P.W. Czoty, H.R. Smith, P.M. Epperly, L.K. Galbo, Cortical excitability in a nonhuman primate model of TMS, Brain Stimul. 14 (2021) 19–21, https://doi.org/10.1016/j.brs.2020.10.008.

[20] S.N. Kukke, R.W. Paine, C. Chao, A.C. de Campos, M. Hallett, Efficient and reliable characterization of the corticospinal system using transcranial magnetic stimulation, J. Clin. Neurophysiol. 31 (2014) 246–252, https://doi.org/10.1097/WNP.0000000000000057.

[21] J.-M. Therrien-Blanchet, M.C. Ferland, M.-A. Rousseau, M. Badri, E. Boucher, A. Merabtine, L.H. Hofmann, H. Théoret, Stability and test–retest reliability of neuronavigated TMS measures of corticospinal and intracortical excitability, Brain Res. 1794 (2022) 148057, https://doi.org/10.1016/j.brainres.2022.148057.

[22] H.-M. Chen, C.C. Chen, I.-P. Hsueh, S.-L. Huang, C.-L. Hsieh, Test-retest reproducibility and smallest real difference of 5 hand function tests in patients with stroke, Neurorehabilitation Neural Repair 23 (2009) 435–440, https://doi.org/10.1177/1545968308331146.

[23] M.-T. Forster, M. Limbart, V. Seifert, C. Senft, Test-retest reliability of navigated transcranial magnetic stimulation of the motor cortex, Neurosurgery 10 (Suppl 1) (2014) 51–55, https://doi.org/10.1227/NEU.0000000000000075, discussion 55-56.

[24] S. Cermak, Q. Meng, K. Peng, S. Baldwin, C.A. Mejías-Aponte, Y. Yang, H. Lu, Focal transcranial magnetic stimulation in awake rats: enhanced glucose uptake in deep cortical layers, J. Neurosci. Methods 339 (2020) 108709, https://doi.org/10.1016/j.jneumeth.2020.108709.

[25] D.A. Spampinato, J. Ibanez, L. Rocchi, J. Rothwell, Motor potentials evoked by transcranial magnetic stimulation: interpreting a simple measure of a complex system, J. Physiol. 601 (2023) 2827–2851, https://doi.org/10.1113/JP281885.

[26] P.M. Rossini, D. Burke, R. Chen, L.G. Cohen, Z. Daskalakis, R. Di Iorio, V. Di Lazzaro, F. Ferreri, P.B. Fitzgerald, M.S. George, M. Hallett, J.P. Lefaucheur, B. Langguth, H. Matsumoto, C. Miniussi, M.A. Nitsche, A. Pascual-Leone, W. Paulus, S. Rossi, J.C. Rothwell, H.R. Siebner, Y. Ugawa, V. Walsh, U. Ziemann, Non-invasive electrical and magnetic stimulation of the brain, spinal cord, roots and peripheral nerves: basic principles and procedures for routine clinical and research application. An updated report from an I.F.C.N. Committee, Clin. Neurophysiol. 126 (2015) 1071–1107, https://doi.org/10.1016/j.clinph.2015.02.001.

[27] S. Frey, R. Comeau, B. Hynes, S. Mackey, M. Petrides, Frameless stereotaxy in the nonhuman primate, Neuroimage 23 (2004) 1226–1234, https://doi.org/10.1016/j.neuroimage.2004.07.001.

[28] D.L. Adams, J.R. Economides, C.M. Jocson, J.C. Horton, A biocompatible titanium headpost for stabilizing behaving monkeys, J. Neurophysiol. 98 (2007) 993–1001, https://doi.org/10.1152/jn.00102.2007.

[29] E. Kallioniemi, P. Julkunen, Alternative stimulation intensities for mapping cortical motor area with navigated TMS, Brain Topogr. 29 (2016) 395–404, https://doi.org/10.1007/s10548-016-0470-x.